On the feasibility of affordable high-fidelity CFD simulations for indoor environment design and control

N. Morozova*, F.X. Trias, R. Capdevila, C. D. Pérez-Segarra and A. Oliva

Heat and Mass Transfer Technological Center (CTTC),
Universitat Politècnica de Catalunya - BarcelonaTech (UPC)
ESEIAAT, C/ Colom 11, 08222 Terrassa (Barcelona), Spain
Corresponding author: nina@cttc.upc.edu*

Abstract

Computational fluid dynamics (CFD) is a reliable tool for indoor environmental applications. However, accurate CFD simulations require large computational resources, whereas significant cost reduction can lead to unreliable results. The high cost prevents CFD from becoming the primary tool for indoor environmental simulations. Nonetheless, the growth in computational power and advances in numerical algorithms provide an opportunity to use accurate and yet affordable CFD. The objective of this study is to analyze the feasibility of fast, affordable, and high-fidelity CFD simulations for indoor environment design and control using ordinary office computers. We analyze two representative test cases, which imitate common indoor airflow configurations, on a wide range of different turbulence models and discretizations methods, to meet the requirements for the computational cost, run-time, and accuracy. We consider statistically steady-state simulations for indoor environment design and transient simulations for control. Among studied turbulence models, the no-model and large-eddy simulation with staggered discretizations show the best performance. We conclude that high-fidelity

CFD simulations on office computers are too slow to be used as a primary tool for indoor environment design and control. Taking into account different laws of computer growth prediction, we estimate the feasibility of high-fidelity CFD on office computers for these applications for the next decades.
Keywords: Computational Fluid Dynamics, Transient Simulations, Turbulence Modeling, Natural Convection, Mixed Convection, Real-Time Simulations

1. Introduction

Heating ventilation and air conditioning (HVAC) systems account for approximately 40% of the energy consumption in buildings [1], which can be decreased by proper design and precise control of indoor air parameters. Therefore, the fast computation of indoor airflow is required for testing different design options or performing model predictive control (MPC) using real-time weather and occupant's behavior data. Nowadays, air distribution in buildings is usually evaluated by multizone models [2], zonal models [3], and computational fluid dynamics (CFD). Multizone models are the most popular choice due to the low computational cost, but they have limited applicability because each room is represented by only one node. Zonal models are considered intermediate between multizone and CFD, however, they usually suffer from case dependency. In CFD, the physical domain is divided into a finite number of control volumes to solve the Navier-Stokes equations numerically. The solution provides a complete set of air parameters for each control volume.

Its high computational cost prevents CFD from becoming the primary

design tool, and it is mostly used for particular high-end buildings. To become a primary design tool, CFD is required to provide sufficient accuracy in capturing flow properties, be fast, and fit into an office computer. The indoor airflow is usually a multi-scale problem requiring fine computational grids [4]. Moreover, the majority of indoor airflows are turbulent. The effect of turbulence can be accurately resolved using direct numerical simulation (DNS) or modeled using large-eddy simulation (LES) or Reynolds average Navier-Stokes (RANS) approaches. LES models are computationally more expensive than RANS, and both methods have a lower computational cost than DNS.

CFD has been successfully used for detailed simulations of building airflows by many researchers [5, 6, 7, 8, 9]. Nevertheless, all of these studies show the need for a compromise between computational cost and accuracy. Van Hooff *et al.* [5] performed CFD simulations of a generic isolated building. They used a computational grid of 5×10^6 control volumes to achieve reliable results, which required to use 14 CPU cores on a high-performance computer. Other studies also indicate the high computational cost of CFD. For example, Chen *et al.* [7] showed that an accurate simulation of a kitchen room would require at least 10^6 control volumes. Chen *et al.* [6] used a grid of 4×10^6 control volumes for an accurate simulation of an office room with a ceiling fan. Zheng *et al.* [9] studied the wind flow for buildings with balconies using a fine mesh of 2×10^7 cells. An ordinary office computer does not have sufficient memory and CPU power to complete such large simulations in a reasonable amount of time for indoor environment design and control. Moreover, the widely used RANS turbulence models do not always produce

satisfactory results, making the use of more accurate (and more expensive) turbulence models indispensable [5, 9].

Accurate CFD simulations require large computational resources, while using ordinary office computers can result in unreasonably long run-times. Grid coarsening and RANS turbulence modeling are common ways to reduce the cost of CFD, but they can lead to overly inaccurate results. Therefore, the task of performing affordable yet accurate CFD is not straightforward.

Over the last decade several attempts to reduce the computational cost of CFD for indoor environmental applications have been made. Wang & Zhai [10] examined the credibility of coarse-grid CFD for HVAC applications and optimized the space discretization to reduce the total truncation error. Kempe & Hantsch [11] applied the immersed boundary method to an LES simulation of a room with a heat source and achieved real-time LES simulations with 32 CPU cores. However, they did not provide an extensive error analysis to evaluate the accuracy of the simulations. Moreover, they did not study the transient flows and did not consider different turbulence models. As an alternative to CFD, the lattice Boltzmann method (LBM) [12, 13, 14] and fast fluid dynamics (FFD) [15, 16] were applied for indoor environmental simulations. LBM time step is limited by the advection term, which makes it slower than CFD with similar grid resolutions [13]. Zuo & Chen [16] adapted FFD for airflow in buildings and introduced turbulence modeling. FFD has lower computing cost but also lower accuracy than CFD [16].

Another important application is the indoor environment control. MPC elaborates a model of the system evolution and executes control actions based on it [17]. Usually, low order models such as multizone, are used

in MPC [18, 19]. So far CFD has not been integrated into MPC directly due to the huge computational cost and nonlinearity of the governing equations. However, several preliminary attempts have been made to simplify CFD to fit MPC requirements [20, 21]. The growth in computational power provides an opportunity to test the feasibility of CFD for MPC. Typically, building MPC systems have a control horizon of 4-5 hours [22], which is relatively short for building dynamics scale, thus transient simulations are required. Moreover, CFD simulations for MPC should be faster than real-time and computationally affordable.

The objective of this work is to study the feasibility of affordable high-fidelity CFD for indoor environmental applications. We consider two representative cases, namely, a tall differentially-heated cavity and a ventilated cavity with a heated floor. We test both cases on a wide range of staggered and collocated grids with different LES, RANS, and DNS approaches. Performed CFD simulations are analyzed in terms of computational cost and accuracy in order to meet the requirements for indoor environmental applications. The work is primarily focused on steady CFD for design and transient CFD for MPC in buildings, using affordable office computers.

The content of this paper is organized as follows: Section 2 describes the details of the test cases and the governing equations, Section 3 describes the numerical methods, Section 4 shows obtained results and their analysis, Section 5 discusses results and their applications, and Section 6 contains concluding remarks.

2. Governing equations and physical problems

2.1. Governing equations

The incompressible Navier-Stokes equations for a Newtonian fluid with constant physical properties are considered. The Boussinesq approximation is adopted to account for the density variations due to temperature difference. Thermal radiation is neglected. Under these assumptions, the governing equations are

$$\nabla \cdot \mathbf{u} = 0, \tag{1}$$

$$\frac{\partial \mathbf{u}}{\partial t} + (\mathbf{u} \cdot \nabla)\mathbf{u} = \nu \nabla^2 \mathbf{u} - \nabla p + \beta \mathbf{g} \Delta T, \tag{2}$$

$$\frac{\partial T}{\partial t} + (\mathbf{u} \cdot \nabla)T = \alpha \nabla^2 T, \tag{3}$$

where $\mathbf{u} = (u, v, w)$ is the velocity vector in Cartesian coordinates $\mathbf{x} = (x, y, z)$, p the kinematic pressure, T the temperature, ν the kinematic viscosity, ρ the density, $\mathbf{g}$ the gravitational acceleration, β the thermal expansion coefficient and α the thermal diffusivity.

Hereafter, all the results are presented in dimensionless form. The reference values of time velocity temperature and length are specified for each problem separately.

2.2. Test case 1: Differentially heated cavity

The first test case is a three-dimensional tall cavity driven by buoyancy forces. The objective of this configuration is to mimic a highly stratified turbulent indoor environment with natural convection. This airflow can be found in a tall building atrium, or a staircase. Natural convection is important for the thermal comfort, thus, its correct prediction is crucial for building

applications. The cavity has a height aspect ratio of $A_h = H/L = 3.84$ and a depth aspect ratio of $A_d = D/L = 0.86$ (Figure 1, left). The Prandtl number corresponds to air and is equal to $Pr = \nu/\alpha = 0.71$ and the Rayleigh number is $Ra = \rho g \beta \Delta T H^3/(\nu\alpha) = 1.2 \times 10^{11}$. This configuration resembles the experimental set-up performed by Saury *et al.* [23]: the two opposite vertical walls of the cavity in the x direction are maintained at uniform temperatures $T_h = 0.5$ at $x = 0$ and $T_c = -0.5$ at $x = L$. The temperature at the rest of the walls is given by the "Fully Realistic" boundary conditions proposed in [24]. They are time independent analytical functions that fit the experimental data obtained by Salat *et al.* [25].

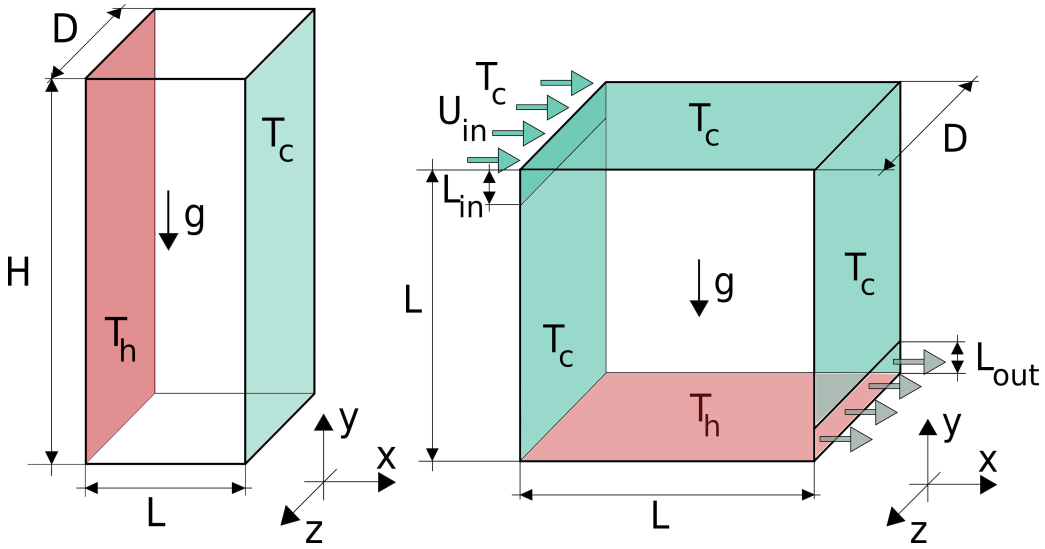

Figure 1: Left: geometry of the differentially heated cavity case. Right: geometry of the mixed convection case.

In the experiment by Saury *et al.* [23] the cavity is 3.84 m high, 1 m wide, 0.86 m deep and is exposed to a temperature difference of $\Delta T = 20°C$. The air properties are the following: $\nu = 1.51 \times 10^{-5} m^2/s$, $\alpha = 2.13 \times 10^{-5} m^2/s$,

$\rho = 1.2kg/m^3$, $g = 9.81m/s^2$ and $\beta = 2.90 \times 10^{-3}m^3/(kg°C)$.

For this test case the reference length is H and the reference velocity, time and temperature used for the dimensionless form are, respectively, $Ra^{1/2}(\alpha/H)$, $Ra^{-1/2}(H^2/\alpha)$ and ΔT. Initial temperature conditions repeat the temperature profile of the front/rear wall boundaries. The initial velocity is set to zero.

Case	N_x	N_y	N_z	N_{total}
M1.0 (DNS)	450	900	256	1.04×10^8
M1.1	8	30	4	9.60×10^2
M1.2	10	40	6	2.40×10^3
M1.3	12	50	8	4.80×10^3
M1.4	14	60	10	8.40×10^3
M1.5	18	80	12	1.73×10^4
M1.6	24	100	16	3.84×10^4
M1.7	30	120	20	7.20×10^4
M1.8	40	150	24	1.44×10^5
M1.9	50	180	30	2.70×10^5
M1.10	70	240	40	6.72×10^5
M1.11	80	320	50	1.28×10^6
M1.12	100	400	60	2.40×10^6

Table 1: Computational grids used in the simulations of the differentially heated cavity case (test case 1).

As detailed in Table 1, we used twelve different Cartesian structured grids for the numerical tests. Grid M1.0 was used in the reference DNS

simulation, which was previously published in Álvarez *et al.* [26]. All the grids are, uniform in the vertical (y) and spanwise (z) directions, and refined near the lateral walls (x) using the hyperbolic tangential function:

$$x = \frac{L}{2}\left(1 + \frac{\tanh\gamma_x(2(i-1)/N_x - 1)}{\tanh\gamma_x}\right), \tag{4}$$

where the concentration factor is $\gamma_x = 2$ and N_x is the number of grid points in the horizontal direction. All steady simulations run for 600 non-dimensional time units, which was found to be a long enough time-integration period to record the flow statistics for further averaging. All transient simulations were carried out for 10 non-dimensional time units to capture the initial flow development.

2.3. Test case 2: Mixed convection in a ventilated cavity

The second test case is a three-dimensional ventilated cavity with a heated floor. This configuration was first studied experimentally by Blay *et al.* [27] and later numerically by Ezzouhri *et al.* [28]. The geometry of the studied cavity is shown in Figure 1 (right). The height aspect ratio of the cavity is $A_h = L/L = 1$ and the depth aspect ratio is $A_d = D/L = 0.3/1.04$. Cold air at $T_c = -0.5$ enters the cavity through the long thin inlet at the top of the left wall. The inlet velocity profile in the vertical (y) direction corresponds to a parabolic Poiseuille flow with a bulk velocity $U_{in} = 1$. The inlet slot has an aspect ratio $A_{in} = L_{in}/L = 0.018/1.04$. The air is discharged through the outlet with an aspect ratio $A_{out} = L_{out}/L = 0.024/1.04$ at the bottom of the right wall of the cavity. The bottom wall is maintained at a hot temperature of $T_h = 0.5$, while the three other sidewalls are kept at the cold temperature

of $T_c = -0.5$. Periodic boundary conditions are used in the spanwise (z) direction.

The cavity is filled with air ($Pr = 0.71$) at Rayleigh number based on the cavity height $Ra = 2.4 \times 10^9$. Froude number based on the inlet height is equal to $Fr_{L_{in}} = U_{in}/\sqrt{\rho g \beta \Delta T L_{in}} = 5.24$, Reynolds number based on the inlet height is $Re_{L_{in}} = U_{in} L_{in}/\nu = 684$. At the outlet, convective boundary conditions ($\partial\phi/\partial t + U_{in}\partial\phi/\partial x = 0$) are imposed for the velocity and temperature. No-slip boundary conditions are applied on the walls. The initial velocity field is set to zero and the initial temperature is set equal to the temperature at the cold wall.

The experimental setup by Blay *et al.* [27] has height and width of 1.04 m and depth of 0.3 m. The inlet slot has a height of 0.018 m and the outlet slot - 0.024 m. The temperature difference is $\Delta T = 20°C$ and the inlet bulk velocity is $U_{in} = 0.57m/s$. The air properties are the following: $\nu = 1.5 \times 10^{-5} m^2/s$, $\alpha = 2.1 \times 10^{-5} m^2/s$, $\rho = 1.2kg/m^3$ and $g = 9.81m/s^2$.

In this test case, the reference values used for non-dimensionalizing are the cavity height L, the time $t_{ref} = L/U_{ref}$, the velocity $U_{ref} = U_{in}$ and the temperature difference ΔT. This flow configuration is a mixed convection phenomenon. It resembles an airflow in a room with mixing ventilation and thermal exhausts. The aspect ratios of the inlet and the outlet are very similar to the real-size rooms.

Cartesian structured grids detailed in Table 2 were used for this test case. All grids are uniform in the spanwise (z) direction. In the horizontal (x) direction grids are refined near the walls using the hyperbolic tangent function given in equation (4) with a concentration factor $\gamma_x = 1.5$. In the

Case	N_x	$N_{outlet} + N_{bulk} + N_{inlet} = N_y$	N_z	N_{total}
M2.0 (DNS)	512	$57 + 398 + 57 = 512$	128	3.36×10^7
M2.1	10	$2 + 10 + 3 = 15$	4	6.00×10^2
M2.2	15	$2 + 20 + 3 = 25$	4	1.50×10^3
M2.3	20	$2 + 25 + 3 = 30$	4	2.40×10^3
M2.4	30	$4 + 32 + 4 = 40$	4	4.80×10^3
M2.5	40	$4 + 32 + 4 = 40$	6	9.60×10^3
M2.6	40	$6 + 48 + 6 = 60$	8	1.92×10^4
M2.7	50	$6 + 48 + 6 = 60$	12	3.60×10^4
M2.8	60	$7 + 60 + 8 = 75$	16	7.20×10^4
M2.9	80	$10 + 70 + 10 = 90$	20	1.44×10^5
M2.10	100	$15 + 90 + 15 = 120$	24	2.88×10^5
M2.11	120	$20 + 120 + 20 = 160$	30	5.76×10^5
M2.12	160	$20 + 140 + 20 = 180$	40	1.15×10^6

Table 2: Computational grids used in the simulations of the mixed convection case (test case 2).

vertical (y) direction the grids are uniform in the zones of inlet (N_{in}) and outlet (N_{out}) and refined near the lateral walls in the bulk part ($\gamma_y = 2$). All simulations run for 500 and 10 non-dimensional time units, respectively for steady and transient cases.

3. Numerical methods

We use three different software to perform the simulations:

- OpenFOAM v1706 [29] for unsteady RANS (URANS) approach using finite-volume discretization on collocated grids with fully implicit Euler time integration scheme;
- TermoFluids [30], an in-house CFD code for LES and no-model approaches using symmetry-preserving finite-volume discretization on collocated grids [31] with a one-parameter fully explicit second-order temporary discretization scheme [32];
- STG [33, 34], an in-house CFD code for LES, DNS and no-model simulations using symmetry-preserving finite volume discretization on staggered grids [35] with a one-parameter fully explicit second-order temporary discretization scheme [32].

The choice of the turbulence models is based on the findings of Morozova *et al.* [36] and Zhai *et al.* [37] for steady simulations and on findings of Morozova *et al.* [38] for transient simulations.

3.1. Unsteady Reynolds-averaged Navier-Stokes approach

The RANS approach is based on the time-averaged filtering of the governing equations (1) - (3). RANS equations calculate only averaged flow; thus,

they are not suitable to describe the transient flow evolution. For this reason, the URANS approach is adopted. URANS equations are obtained when the temporal derivative of velocity is averaged over a chosen finite time. More details on the URANS can be found in [39]. The computational time of the URANS approach is smaller than LES or DNS, hence it is widely used for industrial applications. However, URANS does not always provide sufficient accuracy for the simulations. Nevertheless, it is interesting to test URANS models, as they offer computational time reduction.

In this study three different RANS turbulence models are tested: $k-\epsilon$ [40], RNG $k-\epsilon$ [41] and SST $k-\omega$ [42]. During the numerical experiments, the SST $k-\omega$ model showed the best transient predictions among all the URANS models, but the $k-\epsilon$ model has given better results for the steady flow. The RNG $k-\epsilon$ and $k-\epsilon$ models showed similar performance in terms of accuracy, but the $k-\epsilon$ model had a lower computational cost. Thus, the $k-\epsilon$ and SST $k-\omega$ models are chosen for further analysis. Results of the simulations with the RNG $k-\epsilon$ model are published online in the data archive [43].

3.2. Large-eddy simulation approach

A different approach to turbulence modeling is LES. Namely, the large scale turbulent motions are resolved, whereas the effects of the smallest-scale motions are modeled using a subgrid-scale (SGS) model. In this work three different SGS models are tested: the WALE model [44], the VMS-WALE [45], the QR [46] and the S3PQ model [47]. In terms of computational cost, LES lies between URANS and DNS. Since the large-scale unsteady motions are represented explicitly, LES can be expected to be more accurate and reliable than URANS for flows in which large-scale unsteadiness is significant, in-

cluding unsteady separation and vortex shedding [48]. In this work, we carry out the spatial discretization in LES simulations using symmetry preserving discretization on structured collocated [31] and staggered [35] Cartesian grids.

In a staggered grid discretization arrangement, the scalar variables are stored at the cell centers of the control volumes, whereas the vector variables are stored at the cell faces. In a collocated grid discretization, on the other hand, all variables are stored at the cell centers. A staggered grid discretization helps to avoid odd-even decoupling between the pressure and velocity (a discretization error, which leads to unphysical pressure fields). However, the implementation of the staggered arrangement on the unstructured grids could be extremely complex [31]. Thus, the majority of the common CFD codes use collocated grids with special numerical treatments, which, however, cause considerable numerical dissipation [49]. Nonetheless, many HVAC problems do not require an unstructured grid, therefore, they could be easily used with a staggered grid discretization. This could improve simulation accuracy and reduce numerical dissipation [31, 35] since staggered methods do not require any special numerical treatment. Discretization methods can have an important effect on the simulation stability and the accuracy of the results, especially for the coarsest grids. This reduction of the artificial numerical dissipation is not relevant for RANS models because the dissipation introduced by the model itself is much larger [49]; therefore, staggered grid discretization is only applied to LES and no-model approaches.

LES models tested on collocated grids are WALE, VMS-WALE, and QR. For both test cases, WALE and QR show similar computational cost, but

the VMS-WALE is more expensive due to the additional filtering operations. However, the QR model under-predicted overall heat transfer. For these reasons, we choose the WALE model for further tests. Results of the simulations for the VMS-WALE and QR models are published in the data archive [43]. WALE, QR and, S3PQ turbulence models are tested on structured staggered grids. All three LES models showed similar results, but the WALE had the highest computational cost, and the QR showed the least accurate results. The S3PQ model is chosen for further simulations. Results for the WALE and QR models are published in the online data archive [43].

3.3. No-model approach

The no-model approach is similar to DNS, which consists of solving the Navier-Stokes equations, resolving all the scales of motion [48]. Conceptually DNS is the simplest approach and it is unrivaled in accuracy. However, the cost is extremely high; and the computer requirements increase so rapidly with Reynolds number that the applicability of the approach is very limited even for the research. The no-model approach, like DNS, does not use any model for turbulence. Nonetheless, the computational grid used for no-model simulations is not fine enough to resolve all the turbulent flow scales. Despite the unresolved flow scales, the no-model approach is capable of producing reasonable results. Moreover, the absence of a turbulence model reduces the computational cost.

4. Results and analysis

4.1. Results of the steady-state analysis

The ability for real-time simulations is always a compromise between available computing power and required accuracy. The focus of this paper is on the possibility of real-time CFD on office computers. We performed all the simulations on a machine with an AMD Opteron 2350 processor with a $24Gb/s$ memory bandwidth. Then we re-scaled computational time to Intel Core i9-9900K processor with $41.6Gb/s$ memory bandwidth, which is a modern but affordable processor. CFD codes are usually memory-bound and tend to exhibit irregular access patterns to data [50]. The High-Performance Conjugate Gradient benchmark, proposed by Dongarra *et al.* [50] shows, that the computational performance of CFD applications is mostly limited by a processor's bandwidth. Thus, assuming the ideal behavior of the solvers, we re-scaled all the simulations using linear dependencies of the processor's memory bandwidth and the number of nodes. The indicator to evaluate the performance of the solvers is the time ratio between the computational time, t_{sim}, and physically simulated time, $t_{phy} = t \cdot t_{ref}$. A simulation is faster than real-time when $R < 1$.

$$R = \frac{t_{sim}}{t_{phy}}, \tag{5}$$

To evaluate the overall quality of the simulations, we choose five global flow quantities for comparison: Nusselt number, stratification, kinetic energy, enstrophy, and the temperature of the cavity. They represent basic airflow properties and are relevant to the thermal comfort [51]. Nusselt number, stratification, and temperature represent the thermal properties of the flow.

Nusselt is a measure of heat transfer. It is computed using the temperature gradient at the wall. Stratification corresponds to a vertical temperature gradient, and the average temperature is the operative room temperature. Kinetic energy measures the level of motion. Enstrophy corresponds to turbulence intensity. Both kinetic energy and enstrophy are used to measure draught and local discomfort.

$$Nu = -\frac{1}{A}\int_A \frac{\partial T}{\partial x} dA \quad \text{at} \quad x = 0 \tag{6}$$

$$S = \frac{\partial T}{\partial y} \quad \text{at} \quad x = \frac{L}{2}, \quad y = \frac{H}{2}, \quad z = \frac{D}{2} \tag{7}$$

$$E = \frac{1}{V}\int_V \frac{\mathbf{u}^2}{2} dV \tag{8}$$

$$\Omega = \frac{1}{V}\int_V \omega^2 dV \tag{9}$$

$$T_V = \frac{1}{V}\int_V T dV, \tag{10}$$

where A is the surface of the hot wall, V is the volume of the cavity and $\boldsymbol{\omega} = \nabla \times \mathbf{u}$ is the vorticity. All these quantities are time-dependent, and for the steady-state evaluation they are averaged over time. Standard bracket "<>" notation is used for time-averaged values.

The design of HVAC systems is normally divided into two stages: early conceptual design and final detailed design. In the former, highly accurate simulations are not required. At this stage of a project, only conceptual decisions are made. More important for conceptual design is the ability to have fast calculations. For this design stage, a 15% relative error is assumed acceptable. On the other hand, final stage design applications require accurate and detailed simulation results. Therefore, a relative error of the global quantities should remain below 5%, as it is suggested in [52]. A building project in

many cases requires several representative daily simulations [53]. We assume the simulation speed for HVAC design should be at least twice faster than real-time ($R \leqslant 0.5$) so that an engineer can start a daily simulation at the end of the working day and obtain the results the next morning.

Figures 2 - 6 show global airflow quantities plotted with different grid resolutions and turbulence models against the computational time ratio in a semi-logarithmic scale. Each point of the graph corresponds to a mesh from Tables 1 and 2, respectively. On the left side of the graphs, there are less computationally expensive and less accurate coarse grids with a small ratio R. The mesh resolution is increasing while moving from the left to the right side of the graphs. The thick horizontal black line is the reference value, obtained in the DNS simulations. Gray areas around the reference line show the 5% and 15% error margins, respectively.

4.1.1. Test case 1 - differentially heated cavity. Results of the steady simulations

For this test case we investigate four global quantities: the average Nusselt number, the average stratification, the average kinetic energy and the average enstrophy. We compare them against the DNS data, published in [26].

All the turbulence models except URANS $k-\epsilon$ predict the average Nusselt number (Figure 2, top) rather well. All approaches show small values of $<Nu>$ on coarse grids, but from mesh M1.5 onward, results start falling into the 15% error range. URANS simulations have the least accurate predictions, although their computational cost is the smallest. LES (with both discretization approaches) and no-model on collocated grids show the best results and perform faster than real-time simulations with less than 15% rel-

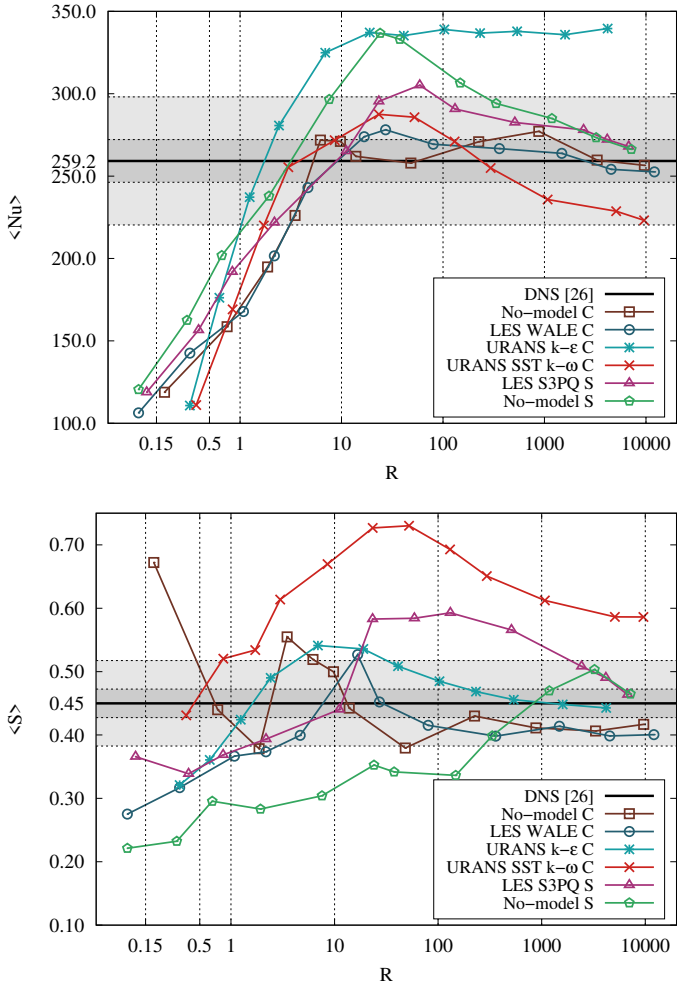

Figure 2: Test case 1. Steady-state analysis. Average Nusselt number (top) and average stratification (bottom) on different grid resolutions and turbulence models against time ratio. Each point in the graph corresponds to a mesh from Table 1. "C" stands for collocated grid discretization and "S" - for staggered.

ative error. Average stratification (Figure 2, bottom) shows good accuracy for most of the approaches. The errors are mostly originating from the fact that it is not an integral quantity. Both no-model techniques predict strat-

ification accurately. URANS $k-\epsilon$ model is giving an accurate prediction, while SST $k-\omega$ is experiencing errors. Both LES simulations perform faster than real-time with about 15% relative error.

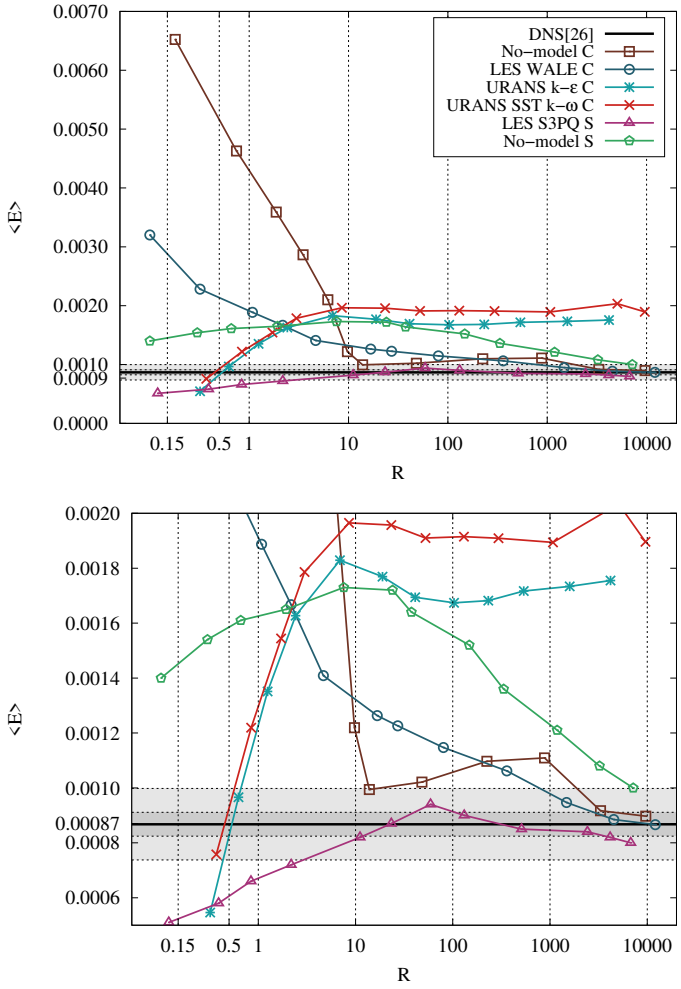

Figure 3: Test case 1. Steady-state analysis. Top: Average kinetic energy against time ratio. Bottom: Zoomed image of the graph at the top. Labeling is the same as in figure 2.

Average kinetic energy (Figure 3) is well predicted only by the LES-S3PQ model on staggered grids. Relatively small values of kinetic energy make its

correct prediction more difficult. LES-WALE and both no-model approaches have converged to the DNS solution only for the finest meshes (M1.11 and M1.12 from Table 1), and URANS failed to predict average kinetic energy correctly for all the mesh resolutions. None of the methods achieves faster than real-time performance with required accuracy.

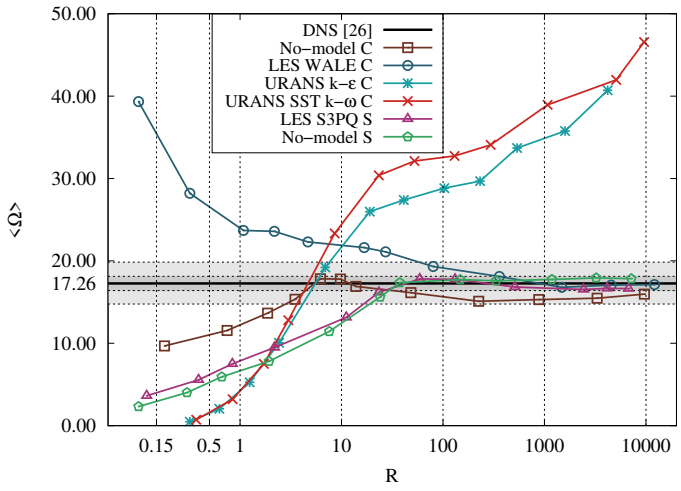

Figure 4: Test case 1. Steady-state analysis. Average enstrophy against time ratio. Labeling is the same as in figure 2.

Average enstrophy (Figure 4) is a characteristic of turbulence cascade, so it is the most difficult quantity to predict accurately. No-model and LES methods provide sufficiently accurate results, however, they are not faster than real-time. Both URANS models, on the other hand, fail to give accurate values of the enstrophy. A significant difference in the accuracy of the results is due to the nature of turbulence modeling. Unlike the other approaches, URANS does not solve the turbulent fluctuations in time, which is the reason for its low accuracy.

From the simulation results could be concluded that, despite the lowest computational cost, URANS simulations have the least accurate predictions of the averaged global quantities of the differentially-heated cavity test case. Both LES models show similar levels of accuracy. No-model simulations on collocated grids show large errors on coarse grids. On the other hand, no-model approach on staggered grids has more stable behavior than the collocated discretization. On fine grids, no-model and LES approaches provide similar results. In general, the LES-S3PQ model on staggered grids shows the best trade-off between computational cost and accuracy for the steady-state analysis of the differentially-heated cavity test case. It reaches the desired accuracy of 15% and 5% with time ratios of $R \approx 25$ and $R \approx 60$, respectively. The least accurate prediction is provided by the URANS SST $k - \omega$ model. Nusselt number appears to be the easiest quantity to predict, while enstrophy is the most difficult one.

4.1.2. Test case 2 - mixed convection. Results of the steady simulations

For this test case, we use three global quantities: the average temperature, the average kinetic energy, and the average enstrophy. We compare them against the DNS data (published in the data archive in [54]), obtained using the in-house STG code described in section 3.2. In this case, we use a fourth-order symmetry preserving discretization scheme [35].

Averaged temperature (Figure 5) is well predicted by all of the approaches. Even the coarsest meshes fall within a 15% error range and perform faster than real-time simulations. The temperature field appears to be relatively easy to predict since it is an integral quantity, which mostly depends on the energy balance.

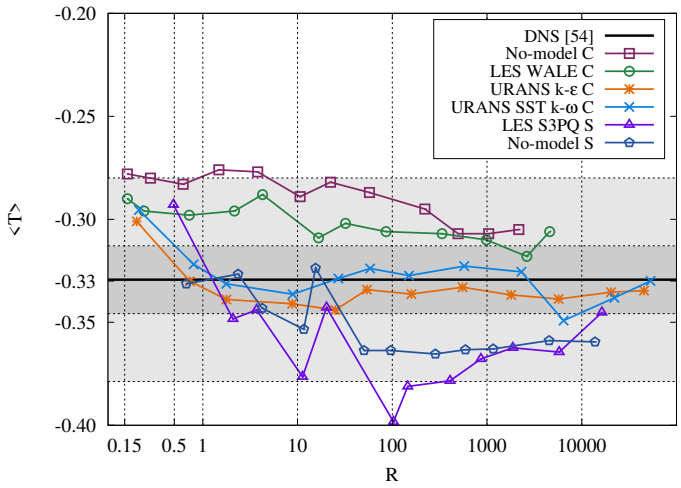

Figure 5: Test case 2. Steady-state analysis. Average temperature with different grid resolutions and turbulence models against time ratio. Each point in the graph corresponds to a mesh from Table 2. "C" stands for collocated grid discretization and "S" - for staggered.

Average kinetic energy (Figure 6, top) is more difficult to calculate correctly. Even though none of the models show very large errors, they are far from the DNS solution. The specific geometry of the test case makes the accurate resolution of the jet possible only with sufficiently fine spatial grid near the inlet area. Nonetheless, all the approaches show positive convergence tendency towards the reference value of kinetic energy. Enstrophy (Figure 6, bottom) is reasonably well predicted by the LES and no-model approaches, however, the computational speed is slower than real-time. URANS models show incorrect results, which could be explained by the nature of the turbulence modeling in URANS.

This test case is more difficult to be solved accurately due to the small aspect ratios of the inlet and outlet openings. Figure 7 features a snapshot

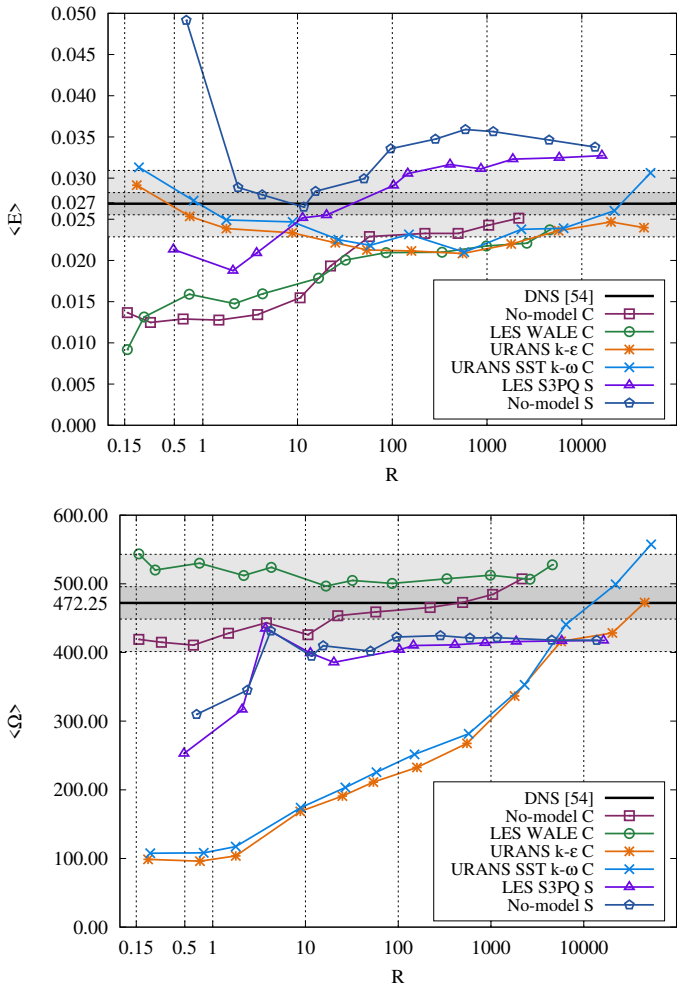

Figure 6: Test case 2. Steady-state analysis. Average kinetic energy (top) and average enstrophy (bottom) against time ratio. Labeling is the same as in figure 5.

360 from a video [54] of the DNS simulations with different mesh resolutions. The quantity plotted in the snapshot is the velocity magnitude. It is seen in the figure how the mesh resolution affects the prediction of the jet shape. Results for the finest mesh show a well-defined jet, which separates from the ceiling near the right wall. As the mesh resolution decreases, the jet appears

to look more distorted and the separation point moves away from the right wall.

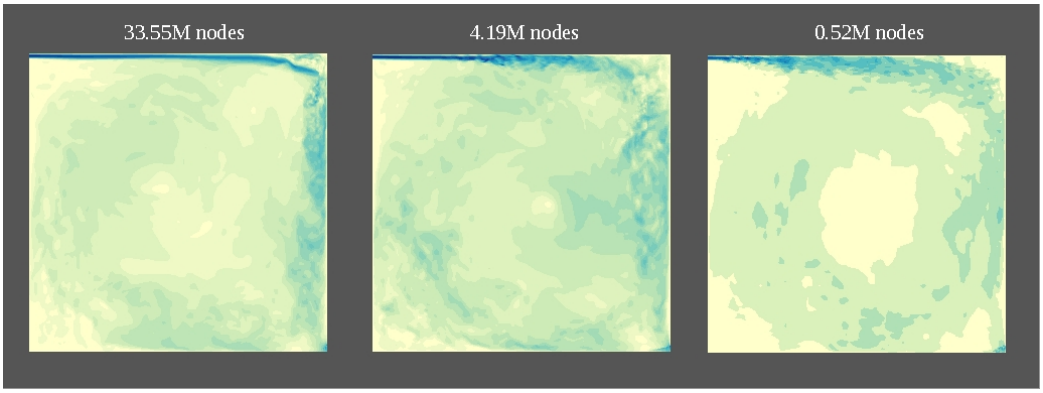

Figure 7: Snapshot from a video of the DNS simulations of the mixed convection case (test case 2). The plotted quantity is the velocity magnitude. The full video is available at [54]

.

As seen in the Figures 5-6, the no-model and LES approaches give similar results, but the no-model on staggered grids shows the best performance for the steady-state analysis. It reaches the desired accuracy of 15% and 5% with the time ratios of $R \approx 4$ and $R \approx 13810$, respectively. The least accurate predictions are provided by the URANS models. The average cavity temperature appears to be the easiest quantity to predict, while enstrophy is the most difficult one.

4.2. Results of the transient analysis

This section presents the analysis of the transient simulations of the same test cases. The purpose of the analysis is to study the feasibility of CFD for MPC of indoor air parameters. In MPC for buildings the prediction is usually

made for the next 4-5 hours with the time step of 1-3 hours [22]. Therefore, for the worst-case scenario the CFD for MPC should be at least 6 times faster than real-time ($R \leq 1/6 \lesssim 0.15$). Transient simulations are re-scaled in the way described in Section 4.1. The same global quantities are considered in the transient analysis. The quality of transient simulations is studied by measuring the dynamic trend using root mean square error (RMSE) of the instantaneous values with respect to the DNS solution. The values of the error are calculated as follows:

$$RMSE(\phi) = \frac{\sqrt{\int_{t_{ini}}^{t_{end}} (\phi - \phi_{DNS})^2 dt}}{\sqrt{\int_{t_{ini}}^{t_{end}} \phi_{DNS}^2 dt}}, \tag{11}$$

where t_{ini} and t_{end} are the beginning and the end of the time integration period respectively, ϕ is the variable of interest, ϕ_{DNS} its value obtained via the DNS simulation. In the next subsections, the results of the two test cases are discussed in detail using the methodology presented above.

4.2.1. Test case 1 - differentially heated cavity. Results of the transient simulations

For the differentially heated cavity case, three global quantities are considered: Nusselt number on the hot wall, kinetic energy, and enstrophy. Stratification was discarded because of its high fluctuations. Simulation results are compared to DNS results previously published in [26]. Time evolution of these quantities is shown in Figures 8-10 (top). Time evolution is plotted for mesh M1.8 (Table 1), as it is the coarsest mesh that provided the desired accuracy. In Figures 8-10 (bottom) the RMSE of these quantities are plotted against the computational time ratio R in logarithmic scale. Each point of

the graph represents a mesh from Table 1. The dashed line separates the area within 15% error from the value of perfect correlation ($RMSE(\phi) = 0$).

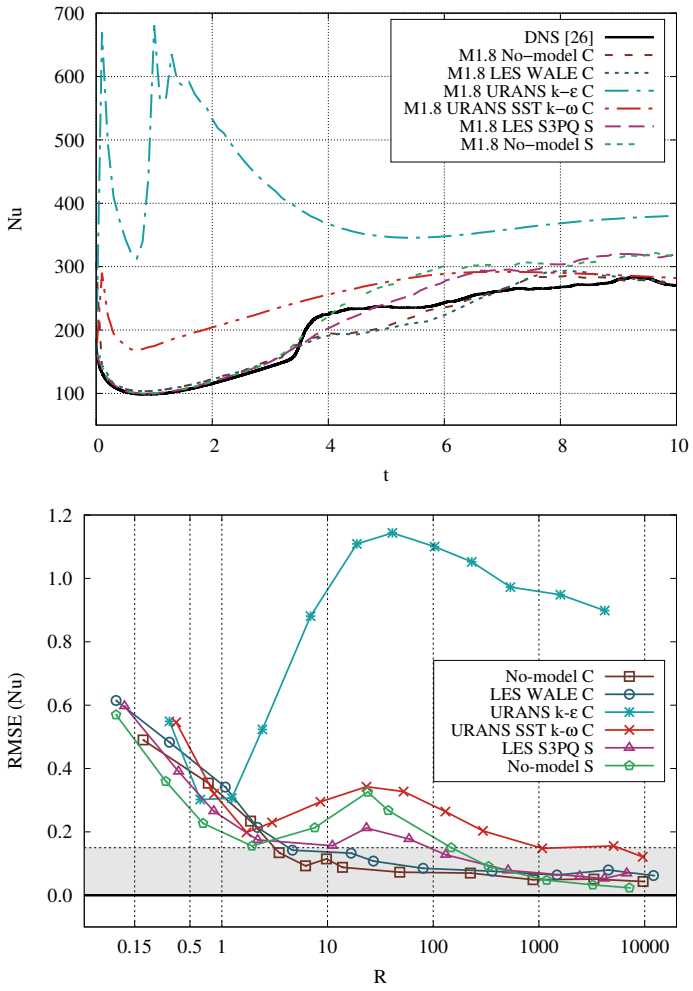

Figure 8: Test case 1. Top: Time evolution of the Nusselt number on the hot wall. Bottom: RMSE of the Nusselt number with different grids and turbulence models against time ratio. Each point in the bottom graph corresponds to a mesh from Table 1. "C" stands for collocated grid discretization and "S" - for staggered.

Nusselt number (Figure 8) is the fastest quantity to converge towards a

steady-state. LES and no-model behave similarly to the reference. URANS $SSTk-\omega$ model also has acceptable dynamic trend. However, URANS $k-\epsilon$ model shows a negative correlation since its transient behavior is completely different from that of DNS.

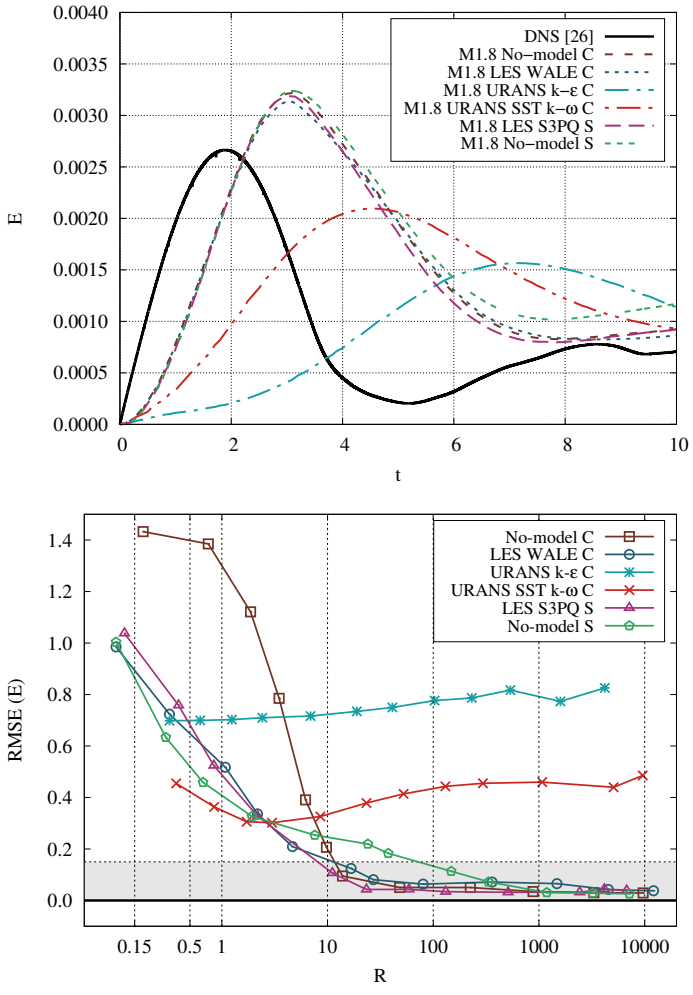

Figure 9: Test case 1. Top: Time evolution of the kinetic energy. Bottom: RMSE of the kinetic energy against time ratio. Labeling is the same as in figure 8.

Reference kinetic energy (Figure 9) shows a good correlation tendency

on LES and no-model approaches (both staggered and collocated discretizations). On the other hand, both URANS models again exhibit a negative tendency because of the late peak. Enstrophy (Figure 10) is showing behavior similar to kinetic energy. URANS results exhibit the peak later than the reference, and this gives low correlation values. LES and no-model approaches show good transient correlation.

For test case 1, the LES and no-model approaches give the best transient correlations, but the LES-S3PQ model on staggered grids has the lowest computational cost. Results for staggered and collocated approaches are very similar, but the staggered discretization has a better correlation at low mesh resolutions. LES and no-model approaches enter 15% error range at mesh resolution M1.8 of the Table 1 with the time ratio $R \approx 130$. The least accurate predictions are provided by the URANS models.

4.2.2. Test case 2 - mixed convection. Results of the transient simulations

For the transient analysis, three global quantities are considered: kinetic energy, enstrophy, and cavity temperature. Time evolution of these quantities is presented in Figures 11-13 (top) and their associated RMSE is plotted against time ratio R in Figures 11-13 (bottom). Again, the DNS simulation is used as a reference [54]. Time evolution is plotted for the mesh M2.12 (Table 2), as no other coarser mesh has reached the desired accuracy.

The mean cavity temperature (Figure 11) is predicted correctly even by very coarse meshes. Both LES and no-model approaches show the smooth convergence aligned with the DNS profile. Although URANS profiles look different from the reference, their prediction error is still within the acceptable margin. LES-S3PQ model on staggered grids has shown the best transient

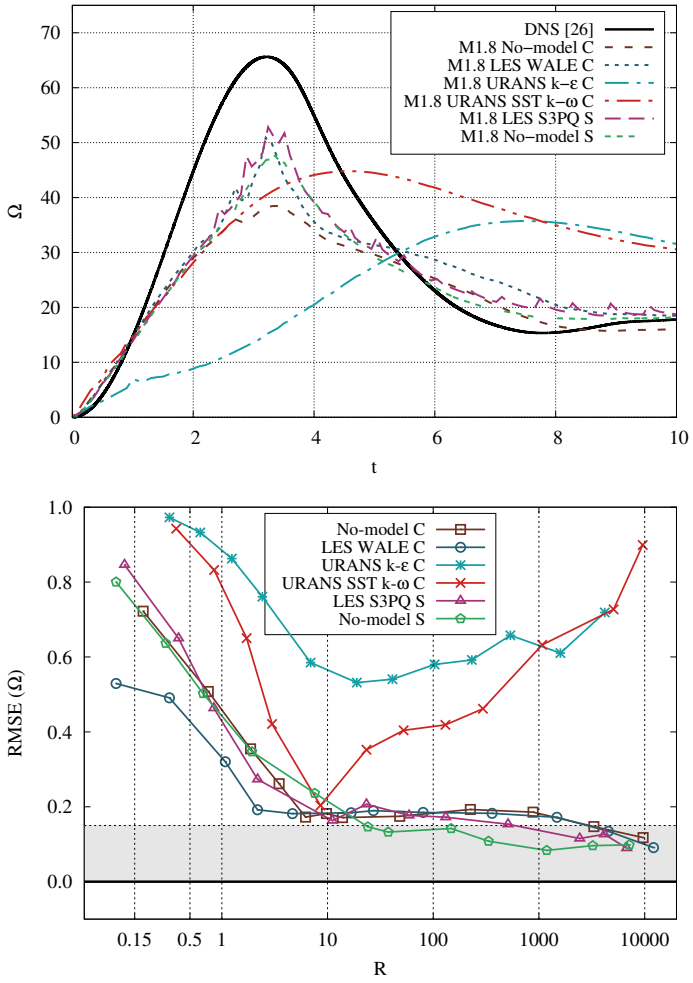

Figure 10: Test case 1. Top: Time evolution of the enstrophy. Bottom: RMSE of the enstrophy against time ratio. Labeling is the same as in figure 8.

correlation.

The time evolution of kinetic energy for the mixed convection is more difficult to predict than temperature (Figure 12). The best prediction is given by LES-S3PQ and no-model methods on staggered grids. Collocated LES and no-model simulation show slower time convergence, and URANS

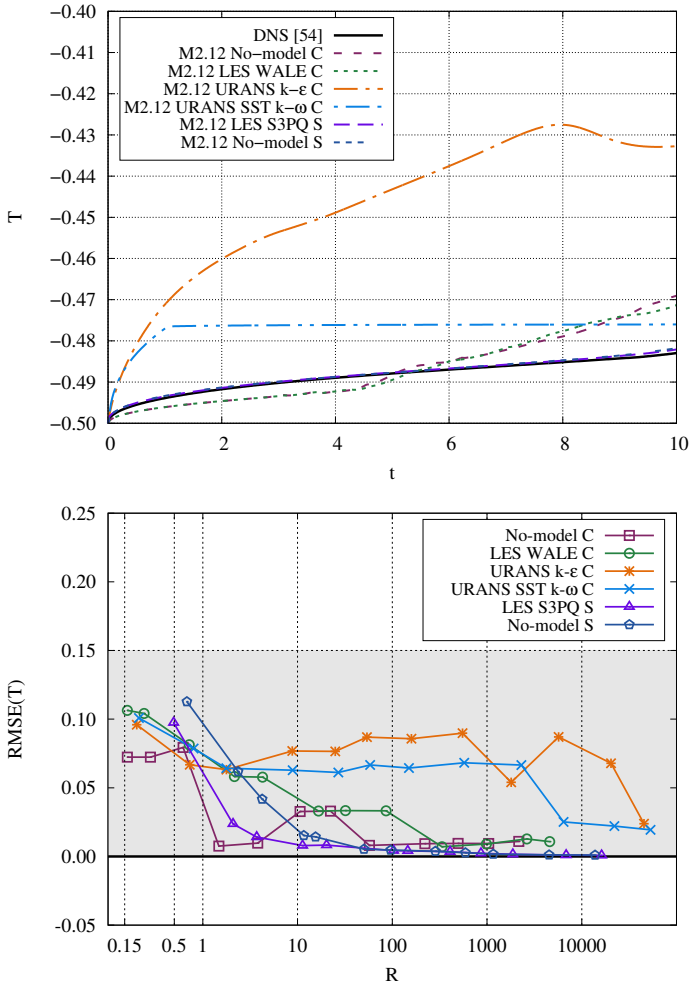

Figure 11: Test case 2. Top: Time evolution of the average cavity temperature. Bottom: RMSE of the average cavity temperature with different grids and turbulence models against time ratio. Each point in the bottom graph corresponds to a mesh from Table 2. "C" stands for collocated grid discretization and "S" - for staggered.

convergence is too fast. For the kinetic energy of the mixed convection case, all six tested approaches show an acceptable transient correlation. Enstrophy (Figure 13) is a highly fluctuating quantity, and it is difficult to predict its

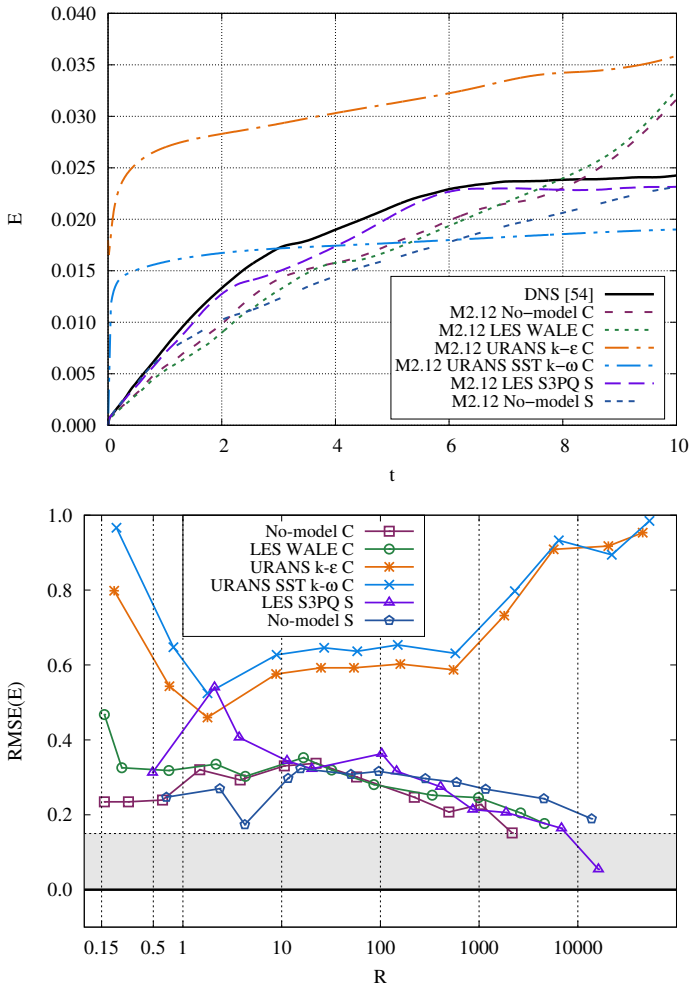

Figure 12: Test case 2. Top: Time evolution of the kinetic energy. Bottom: RMSE of the kinetic energy against time ratio. Labeling is the same as in figure 11.

transient evolution. The behavior of time evolution of the enstrophy is well predicted by LES and no-model simulations, meanwhile, the predictions of URANS are very inaccurate. URANS time evolution is smooth, while other approaches show multiple small peaks. This is demonstrated by the low values of the correlation coefficient for URANS models.

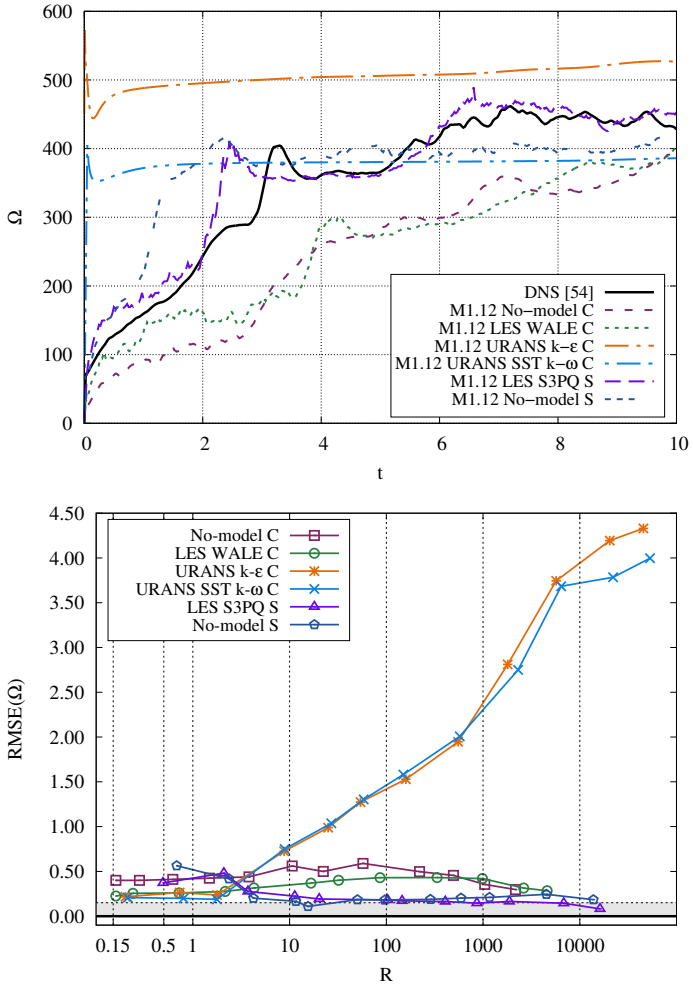

Figure 13: Test case 2. Top: Time evolution of the enstrophy. Bottom: RMSE of the enstrophy against time ratio. Labeling is the same as in figure 11.

435 Even though this test case is less turbulent than the previous one, the complexity of the physics of the problem requires high mesh resolution, which explains the low accuracy of the obtained results. As could be concluded from the results, only the finest mesh M2.12 nears the required accuracy for the transient simulations. The no-model approach on staggered grids gives the

lowest computational cost of $R \approx 13810$ at this mesh resolution.

4.2.3. Summary of the obtained results

Results for both transient and steady simulations, for both test cases, are summarized in the Table 3. The Table shows computational time ratios for both test cases with all approaches used. The time ratios displayed in the table correspond to the coarsest meshes at which the desired accuracy for all the global quantities of interest is achieved. Since several assumptions are made while computing time ratios, their intervals are given instead of the exact values.

As seen in Table 3, required accuracy was not achieved by real-time or faster than real-time simulations, performed by any of the tested approaches for both transient and steady simulations. Kinetic energy and enstrophy appear to be especially difficult to predict. Even though URANS simulations are the least computationally expensive, their accuracy is often insufficient. Moreover, URANS tends to converge to a solution different from the one provided by the DNS reference. This could be explained by the nature of the URANS models, as they are not suitable for the natural convection and mass separation flows because they have been developed mostly for aerodynamic applications, where boundary layers are usually attached or partially attached [48]. The no-model and LES simulations provide similar results, but the computational cost of the no-model approach is approximately 30% lower. Staggered symmetry-preserving discretization considerably improves the accuracy of the results for coarse and extremely coarse grids with the no-model approach. For the LES simulations, the effect of staggered discretization on the results is less notable.

Case		Model					
		LES WALE C	LES S3PQ S	URANS $k-\epsilon$ C	URANS SST $k-\omega$ C	No-model C	No-model S
1	$< 15\%$ error steady (Conceptual design)						
	$< 5\%$ error steady (Detailed design)			×	×		
	$< 15\%$ error transient (MPC)			×	×		
2	$< 15\%$ error steady (Conceptual design)						
	$< 5\%$ error steady (Detailed design)						
	$< 15\%$ error transient (MPC)			×	×		

Notation						
	$R \leqslant 1$	$1 < R \leqslant 10$	$10 < R \leqslant 100$	$100 < R \leqslant 1000$	$R > 1000$	Low accuracy

Table 3: Computational time ratios R, obtained for the differentially heated cavity (test case 1) and the mixed convection (test case 2) for several indoor environmental applications and different turbulence models. "C" stands for collocated grid discretization and "S" - for staggered. The shadows of blue from light to dark show computational time ratios from low to high, respectively. The red cross stands for the insufficient accuracy.

5. Discussion

In this section, we present the interpretation of the obtained results by moving from the analyzed test cases to their real-life analogs (a generic closed system and a generic open system). We discuss the computational requirements for the indoor environmental simulations and the feasibility of these simulations.

5.1. Extrapolation to real-size problems

To perform the simulations, we adopted the conditions used in the experiments of Saury *et al.* [23] and Blay *et al.* [27] detailed in Section 2. However, these experimental domain sizes and temperature differences are not realistic for indoor environmental problems. The purpose of this section is to extrapolate the findings (in terms of simulation time and feasibility) to more realistic problems.

As an example of a closed system, we consider a building atrium exposed to an arbitrary summer temperature of $T_{hot} = 27°C$ on one side and maintained at the constant temperature of an air-conditioned building of $T_{cold} = 23°C$ ($\Delta T = 4°C$). Maintaining constant dimensionless Pr and Ra numbers of the differentially heated cavity, and constant air properties, the simulated domain size becomes equal to $1.71 \times 6.57 \times 1.47$ meters. The physical time of the simulation is proportional to the square of the domain size; thus, the time ratios for this case decrease by a factor of 2.93, compared to the simulated case.

According to the results presented in Figures 2 - 4 and 8 - 10 for the differentially-heated cavity test case, the minimal time ratios for conceptual

design, detailed design and MPC are $R \approx 25$, $R \approx 60$ and $R \approx 130$, respectively. These are the minimal time ratios which reached the desired accuracy for all the global quantities (LES-S3PQ turbulence model on staggered grids). Using the aforementioned re-scaling factor, they become equal to $R \approx 10$, $R \approx 20$ and $R \approx 45$, respectively.

A similar procedure could be done for the second test case. We assume a room with the temperature difference of $\Delta T = 4°C$, constant inlet bulk velocity, and constant air properties. Maintaining constant dimensionless Pr, Ra and Fr numbers, the new domain size becomes $1.78 \times 1.78 \times 0.51$ meters. Therefore, the physical time of the simulation is multiplied by a factor of 1.71 (proportional to the domain size). Thus the time ratios for conceptual design, detailed design and MPC are re-scaled from $R \approx 4$, $R \approx 13810$ and $R \approx 13810$ (no-model approach on staggered grids) to $R \approx 3$, $R \approx 8000$ and $R \approx 8000$, respectively.

Re-scaled domain sizes for both test cases are not far from the realistic ones, as a result, we conclude that the computational time of the test cases is of the same order of magnitude as of the real HVAC setups. Therefore, they could be used as an estimation for a generic closed system and generic open system, respectively.

5.2. Availability of steady-state simulations for design applications

We assume reasonable speed for both conceptual and detailed design applications as two times faster than real-time ($R \leqslant 0.5$). We accept the values of 15% relative error for the conceptual design and 5% for the detailed design. The minimal time ratios which reached the desired accuracy for all the global quantities, are $R \approx 10$ and $R \approx 20$ for the early and detailed design

stages of the real-size closed system. On the other hand, the time ratios for a generic open system are $R \approx 3$ and $R \approx 8000$, respectively.

The obtained time ratios of the simulations are significantly higher than the required. The computational cost cannot be further reduced without sacrificing the essential accuracy. Results indicate that fast reliable CFD simulations on office computers are currently not available neither for detailed design nor conceptual design stages. Of course, a high-performance supercomputer can handle these simulations with required time ratio and accuracy. However, large computational resources are usually available only for particular high-end building designs, and not for routine use. Thus, it is interesting to analyze when fast and accurate CFD will be feasible on ordinary office computers.

The most well-known law of computational growth is Moore's law [55]. It states that the number of transistors in a dense integrated circuit would double in about every 18 months. We use it as an rough optimistic prediction. On the other hand, as we mentioned earlier, CFD applications are memory-bound. In other words, their performance depends mostly on the memory bandwidth of the processor. Thus, it is interesting to see how it grows. Yet, there is no law, which could predict the bandwidth growth rate. As an estimation, we derive the growth rate from the increase of the DDR SDRAM capacity between the years 1998 and 2020. Within these 22 years, the DDR SDRAM memory bandwidth has grown approximately 39 times bigger. As a rough pessimistic prediction, we estimate that the memory bandwidth will continue growing at the same rate in the future.

Figure 14 shows the estimated decreasing simulation time ratio due to the

growing computational power over the years for different applications and different growth estimations for a generic closed system (top) and a generic open system (bottom). We extrapolate the possible future values of the time ratio using different prediction laws: solid line - the memory bandwidth growth rate, dashed line - Moore's law, the shadowed area between the lines - intermediate possibilities.

Results in Figure 14 significantly vary between optimistic and pessimistic predictions. According to optimistic prediction, the early design stage simulations will be possible in about 5 years. For the detailed design stage, the optimistic predictions go up to 10 years for a generic closed system and 20 years for a generic open system. Yet, pessimistic predictions have a very different waiting horizon. CFD for the early design stage simulations will be possible in 10-15 years. The guess for the detailed design stage is at least 25 years for a closed system and 60 years for an open one.

5.3. Availability of transient simulations for MPC applications

As mentioned earlier, CFD for MPC should be at least 6 times faster than real-time ($R \lesssim 0.15$). The required simulation accuracy highly depends on the controlled building function. It could be assumed that a 15% error in the prediction of the transient evolution of global quantities is sufficient for civil building applications. The time ratio for a generic closed system is $R \approx 45$, which is the best trade-off between computational cost and accuracy. For open systems like the test case 2 (Figures 11 - 13), the obtained time ratio ($R \approx 8000$) is bigger due to the required high mesh resolution in the jet area.

With the current computational resources, it is not possible to incorporate CFD into the MPC system of a building. However, taking into account the

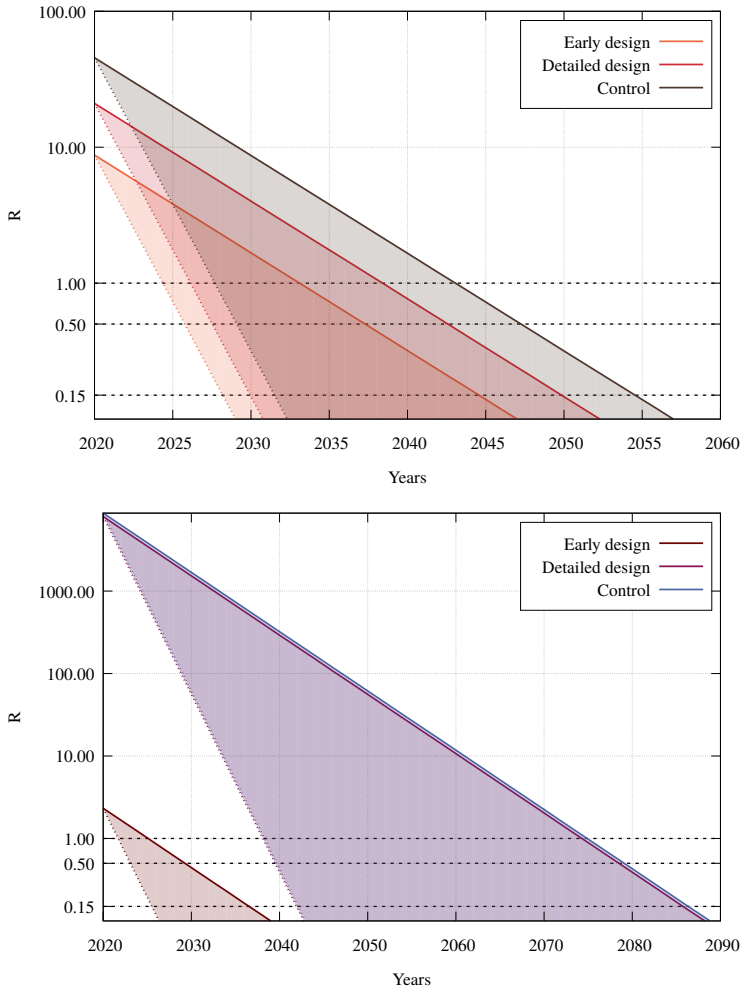

Figure 14: Potential of accessing affordable high-fidelity CFD over the next years. Top: estimation for a generic closed system. Bottom: estimation for a generic open system. The solid line is the memory bandwidth growth rate, and the dashed line is Moore's law growth rate, the shadowed area between the lines - intermediate possibilities.

aforementioned predictions of Moore's law [55] and the bandwidth growth rate, we estimate the time in which transient CFD applications would be available for MPC (Figure 14). The required mesh resolution and the com-

putational resources for different test cases vary significantly. For a closed system based on the differentially heated cavity test case, a good temporal resolution with the required time ratio ($R \lesssim 0.15$) could be achieved within the next 10 years (optimistic prediction). However, an open system based on the mixed convection case needs a higher spatial resolution to perform correct transient simulations, which give us an optimistic prediction of at least 25 years. The pessimistic prediction is showing a very different expected availability - around 35 years for a closed system and around 70 years for an open system with a jet.

The difference between optimistic and pessimistic scenarios is drastic. However, now we can not completely adopt either of them. Probably, at a certain point in the future, a significant technological transformation might occur, which would match the bandwidth growth rate with Moore's law. Alternatively, with the growth of computational performance, more and more applications will become memory-bound, which would shift the further acceleration towards a pessimistic scenario.

6. Conclusions and future work

This work studied the feasibility of affordable, fast, and high-fidelity CFD simulations for indoor environmental applications, considering two representative test cases and a wide range of numerical setups. We considered three possible building applications: conceptual design, detailed design, and MPC.

We tested LES, URANS, and no-model approaches with both staggered and collocated discretizations on a set of structured Cartesian non-uniform grids. LES and no-model approach showed considerably higher accuracy

than URANS. Even though URANS simulations were the least computationally expensive, their accuracy was often insufficient. The no-model approach produces similar to LES results, but with the lower computational cost. Staggered symmetry-preserving discretization considerably improves the accuracy of coarse and extremely coarse grids.

Based on the obtained run-times of the simulations and the building applications requirements, we conclude that, fast high-fidelity CFD simulations on the office computers are not feasible neither for design nor for control of indoor environments. Obtained run-times are too long to make CFD a primary tool for HVAC applications. We estimated the growth of computational resources in the future to determine when CFD would be available for routine use on office computers. The optimistic prediction estimates that CFD would be feasible for conceptual design in 5 years, for the detailed design in 10-20 years, and in 10-25 years for MPC. The pessimistic prediction anticipates at least 15 years for the conceptual design, 25 years for the detailed design, and 35 years for control.

Our findings suggest that the growth of computational resources would not be enough to make CFD available for routine use in building applications. This means more work is required on developing better models and numerical methods, to reduce the computational cost of the simulations while maintaining the accuracy. A possible topic to extend this work is to develop machine learning algorithms based on data from previous CFD simulations, which will be able to correctly predict the quantities of interest with a lower computational cost.

7. Acknowledgments

This work is supported by the Ministerio de Economía y Competitividad, Spain [ENE2017-88697-R]. N. Morozova is supported by the by the Ministerio de Economía y Competitividad, Spain [FPU16/06333 predoctoral contract]. Part of the calculations was performed on the MareNostrum 4 supercomputer at the Barcelona Supercomputing Center [RES project I-2019-2-0021]. The authors thankfully acknowledge these institutions. The authors would also like to thank our colleague MSc Xavier Álvarez Farré for the productive discussions.

References

[1] X. Cao, X. Dai, J. Liu, Building energy-consumption status worldwide and the state-of-the-art technologies for zero-energy buildings during the past decade, Energy and Buildings 128 (2016) 198–213. doi:10.1016/j.enbuild.2016.06.089.

[2] J. Axley, Multizone airflow modeling in buildings: History and theory, HVAC&R Research 13 (6) (2007) 907–928. doi:10.1080/10789669.2007.10391462.

[3] A. C. Megri, H. Fariborz, Zonal modeling for simulating indoor environment of buildings: Review, recent developments, and applications, HVAC&R Research 13 (6) (2007) 887–905. doi:10.1080/10789669.2007.10391461.

[4] Y. Li, P. V. Nielsen, Commemorating 20 years of Indoor Air: CFD and

ventilation research, Indoor Air 21 (6) (2011) 442–453. doi:10.1111/j.1600-0668.2011.00723.x.

[5] T. van Hooff, B. Blocken, Y. Tominaga, On the accuracy of CFD simulations of cross-ventilation flows for a generic isolated building: Comparison of RANS, LES and experiments, Building and Environment 114 (2017) 148–165. doi:10.1016/j.buildenv.2016.12.019.

[6] W. Chen, S. Liu, Y. Gao, H. Zhang, E. Arens, L. Zhao, J. Liu, Experimental and numerical investigations of indoor air movement distribution with an office ceiling fan, Building and Environment 130 (2018) 14–26. doi:10.1016/j.buildenv.2017.12.016.

[7] Z. Chen, J. Xin, P. Liu, Air quality and thermal comfort analysis of kitchen environment with CFD simulation and experimental calibration, Building and Environment 172 (2020) 106691. doi:10.1016/j.buildenv.2020.106691.

[8] E. Katramiz, D. Al Assaad, N. Ghaddar, K. Ghali, The effect of human breathing on the effectiveness of intermittent personalized ventilation coupled with mixing ventilation, Building and Environment 174 (2020) 106755. doi:10.1016/j.buildenv.2020.106755.

[9] X. Zheng, H. Montazeri, B. Blocken, CFD simulations of wind flow and mean surface pressure for buildings with balconies: Comparison of RANS and LES, Building and Environment 173 (2020) 106747. doi:10.1016/j.buildenv.2020.106747.

[10] H. Wang, Z. Zhai, Application of coarse-grid computational fluid dynamics on indoor environment modeling: Optimizing the trade-off between grid resolution and simulation accuracy, HVAC&R Research 18 (5) (2012) 915–933.

[11] T. Kempe, A. Hantsch, Large-eddy simulation of indoor air flow using an efficient finite-volume method, Building and Environment 115 (2017) 291–305. doi:10.1016/j.buildenv.2017.01.019.

[12] F. Kuznik, C. Obrecht, G. Rusaouen, J. J. Roux, LBM based flow simulation using GPU computing processor, Computers & Mathematics with Applications 59 (7) (2010) 2380–2392. doi:10.1016/j.camwa.2009.08.052.

[13] B. Elhadidi, H. E. Khalifa, Comparison of coarse grid lattice Boltzmann and Navier Stokes for real time flow simulations in rooms, Building Simulation 6 (2013) 183–194. doi:10.1007/s12273-013-0107-x.

[14] M. A. I. Khan, N. Delbosc, C. J. Noakes, J. Summers, Real-time flow simulation of indoor environments using lattice Boltzmann method, Building Simulation 8 (2015) 405–414. doi:10.1007/s12273-015-0232-9.

[15] J. Stam, Stable fluids, in: Proceedings of the 26th Annual Conference on Computer Graphics and Interactive Techniques, 1999, pp. 121–128. doi:10.1145/311535.311548.

[16] W. Zuo, Q. Chen, Real-time or faster-than-real-time simulation of air-

flow in buildings, Indoor Air 19 (1) (2009) 33–44. doi:10.1111/j.1600-0668.2008.00559.x.

[17] F. Oldewurtel, A. Parisio, C. N. Jones, D. Gyalistras, M. Gwerder, V. Stauch, B. Lehmann, M. Morari, Use of model predictive control and weather forecasts for energy efficient building climate control, Energy and Buildings 45 (2012) 15–27. doi:10.1016/j.enbuild.2011.09.022.

[18] S. Yang, M. P. Wan, W. Chen, B. F. Ng, D. Zhai, An adaptive robust model predictive control for indoor climate optimization and uncertainties handling in buildings, Building and Environment 163 (2019) 106326. doi:10.1016/j.buildenv.2019.106326.

[19] J. Zhuang, Y. Chen, X. Chen, A new simplified modeling method for model predictive control in a medium-sized commercial building: A case study, Building and Environment 127 (2018) 1–12. doi:10.1016/j.buildenv.2017.10.022.

[20] T. Zerihun Desta, K. Janssens, A. Van Brecht, J. Meyers, M. Baelmans, D. Berckmans, CFD for model-based controller development, Building and Environment 39 (6) (2004) 621–633. doi:10.1016/j.buildenv.2004.01.001.

[21] X. Zhou, H. Li, Y. C. Soh, C. Jiang, Development of a novel strategy of CFD-based model predictive control, Procedia Engineering 214 (2017) 69–75. doi:10.1016/j.proeng.2017.09.821.

[22] A. Afram, F. Janabi-Sharifi, Theory and applications of HVAC control systems - A review of model predictive control (MPC), Building and

Environment 72 (2014) 343–355. doi:10.1016/j.buildenv.2013.11.016.

[23] D. Saury, N. Rouger, F. Djanna, F. Penot, Natural convection in an air-filled cavity: Experimental results at large Rayleigh numbers, International Communications in Heat and Mass Transfer 38 (6) (2011) 679–687. doi:10.1016/j.icheatmasstransfer.2011.03.019.

[24] A. Sergent, P. Joubert, S. Xin, P. Le Quéré, Resolving the stratification discrepancy of turbulent natural convection in differentially heated air-filled cavities Part II: End walls effects using large eddy simulation, International Journal of Heat and Fluid Flow 39 (2013) 15–27. doi:10.1016/j.ijheatfluidflow.2012.10.005.

[25] J. Salat, S. Xin, P. Joubert, A. Sergent, F. Penot, P. Le Quéré, Experimental and numerical investigation of turbulent natural convection in a large air-filled cavity, International Journal of Heat and Fluid Flow 25 (5) (2004) 824–832. doi:10.1016/j.ijheatfluidflow.2004.04.003.

[26] X. Álvarez, A. Gorobets, F. X. Trias, R. Borrell, G. Oyarzun, HPC^2 —A fully-portable, algebra-based framework for heterogeneous computing. Application to CFD, Computers and Fluids 173 (2018) 285–292. doi:10.1016/j.compfluid.2018.01.034.

[27] D. Blay, S. Mergui, J. L. Tuhault, F. Penot, Experimental turbulent mixed convection created by confined buoyant wall jets, in: Proceedings of the First European Heat Transfer Conference, UK, 1992, pp. 821–828.

[28] R. Ezzouhri, P. Joubert, F. Penot, S. Mergui, Large eddy simulation of turbulent mixed convection in a 3D ventilated cavity: Comparison with existing data, International Journal of Thermal Sciences 48 (11) (2009) 2017–2024. doi:10.1016/j.ijthermalsci.2009.03.017.

[29] The OpenFOAM Foundation, OpenFOAM, https://www.openfoam.org/ (2020).

[30] Termo Fluids S.L., Termofluids, http://www.termofluids.com/ (2020).

[31] F. X. Trias, O. Lehmkuhl, A. Oliva, C. D. Pérez-Segarra, R. W. C. P. Verstappen, Symmetry-preserving discretization of Navier-Stokes equations on collocated unstructured grids, Journal of Computational Physics 258 (2014) 246–267. doi:10.1016/j.jcp.2013.10.031.

[32] F. X. Trias, O. Lehmkuhl, A self-adaptive strategy for the time integration of Navier-Stokes equations, Numerical Heat Transfer, Part B: Fundamentals 60 (2) (2011) 116–134. doi:10.1080/10407790.2011.594398.

[33] A. Gorobets, F. X. Trias, M. Soria, A. Oliva, A scalable parallel Poisson solver for three-dimensional problems with one periodic direction, Computers & Fluids 39 (3) (2010) 525–538. doi:10.1016/j.compfluid.2009.10.005.

[34] F. X. Trias, M. Soria, A. Oliva, C. D. Pérez-Segarra, Direct numerical simulations of two- and three-dimensional turbulent natural convection

flows in a differentially heated cavity of aspect ratio 4, Journal of Fluid Mechanics 586 (2007) 259–293. doi:10.1017/S0022112007006908.

[35] R. W. C. P. Verstappen, A. E. P. Veldman, Symmetry-preserving discretization of turbulent flow, Journal of Computational Physics 187 (1) (2003) 343–368. doi:10.1016/S0021-9991(03)00126-8.

[36] N. Morozova, R. Capdevila, F. X. Trias, A. Oliva, Towards real-time CFD simulation of indoor environment, in: Proceedings of 10th International Conference on Computational Fluid Dynamics, 2018.

[37] Z. Zhang, W. Zhang, Z. J. Zhai, Q. Y. Chen, Evaluation of various turbulence models in predicting airflow and turbulence in enclosed environments by CFD: Part-2: Comparison with experimental data from literature, HVAC&R Research 13 (6) (2007) 871–886. doi:10.1080/10789669.2007.10391460.

[38] N. Morozova, R. Capdevila, F. X. Trias, A. Oliva, On the feasibility of CFD for transient airflow simulations in buildings, in: Proceedings of Building Simulation 2019: 16th Conference of IBPSA, 2019.

[39] B. Mikuž, I. Tiselj, URANS prediction of flow fluctuations in rod bundle with split-type spacer grid, International Journal of Heat and Fluid Flow 64 (2017) 10–22. doi:10.1016/j.ijheatfluidflow.2017.01.008.

[40] B. E. Launder, D. B. Spalding, The numerical computation of turbulent flows, Computer Methods in Applied Mechanics and Engineering 3 (2) (1974) 269–289. doi:10.1016/0045-7825(74)90029-2.

[41] V. Yakhot, S. A. Orszag, Renormalization-group analysis of turbulence, Physical Review Letters 57 (14) (1986) 1722–1724. doi:10.1103/PhysRevLett.57.1722.

[42] F. Menter, Two-equation eddy-viscosity turbulence models for engineering applications, AIAA Journal 32 (8) (1994) 1598–1605. doi:10.2514/3.12149.

[43] N. Morozova, F. X. Trias, R. Capdevila, C. D. Pérez-Segarra, A. Oliva, Supplementary material for the journal paper "On the feasibility of CFD simulations for indoor environment design and control", http://www.cttc.upc.edu/downloads/DHC-MC-diffTurbModels/ (2020).

[44] F. Nicoud, F. Ducros, Subgrid-scale stress modelling based on the square of the velocity gradient tensor, Flow, Turbulence and Combustion 62 (1999) 183–200. doi:10.1023/A:1009995426001.

[45] L. Bricteux, M. Duponcheel, G. Winckelmans, A multiscale subgrid model for both free vortex flows and wall-bounded flows, Physics of Fluids 21 (2009). doi:10.1063/1.3241991.

[46] R. W. C. P. Verstappen, When does eddy viscosity damp subfilter scales sufficiently?, Journal of Scientific Computing 49 (1) (2011) 94–110. doi:10.1007/s10915-011-9504-4.

[47] F. X. Trias, D. Folch, A. Gorobets, A. Oliva, Building proper invariants for eddy-viscosity subgrid-scale models, Physics of Fluids 27 (6) (2015). doi:10.1063/1.4921817.

[48] S. B. Pope, Turbulent flows, Cambridge University Press, 2000. doi:10.1017/CBO9780511840531.

[49] E. M. Komen, E. M. Frederix, T. H. Coppen, V. D'Alessandro, J. G. Kuerten, Analysis of the numerical dissipation rate of different Runge–Kutta and velocity interpolation methods in an unstructured collocated finite volume method in OpenFOAM®, Computer Physics Communications 253 (2020) 107145. doi:10.1016/j.cpc.2020.107145.

[50] J. Dongarra, M. A. Heroux, L. P., High-performance conjugate-gradient benchmark: A new metric for ranking high-performance computing systems, The International Journal of High Performance Computing Applications 30 (1) (2015) 3–10. doi:10.1177/1094342015593158.

[51] Ergonomics of the thermal environment — Analytical determination and interpretation of thermal comfort using calculation of the PMV and PPD indices and local thermal comfort criteria, Standard, International Organization for Standardization, Geneva, CH (2005).

[52] F. Ferracuti, A. Fonti, L. Ciabattoni, S. Pizzuti, A. Arteconi, L. Helsen, G. Comodi, Data-driven models for short-term thermal behaviour prediction in real buildings, Applied Energy 204 (2017) 1375–1387. doi:10.1016/j.apenergy.2017.05.015.

[53] O. Neu, S. Oxizidis, D. Flynn, F. Pallonetto, D. Finn, High resolution space - time data: Methodology for residential building simulation

modelling, in: Proceedings of 13th Conference of International Building Performance Simulation Association, 2013, pp. 2428–2435.

[54] N. Morozova, F. X. Trias, R. Capdevila, A. Oliva, Results from a turbulent air-filled ($Pr = 0.71$) mixed convection at $Ra = 2.4 \times 10^9$ and $Fr = 5.24$ (both based on the inlet height), http://www.cttc.upc.edu/downloads/MC_RA2_4e9_FR5_24/ (2020).

[55] G. E. Moore, Cramming more components onto integrated circuits, Proceedings of the IEEE 86 (1) (1998) 82–85. doi:10.1109/jproc.1998.658762.